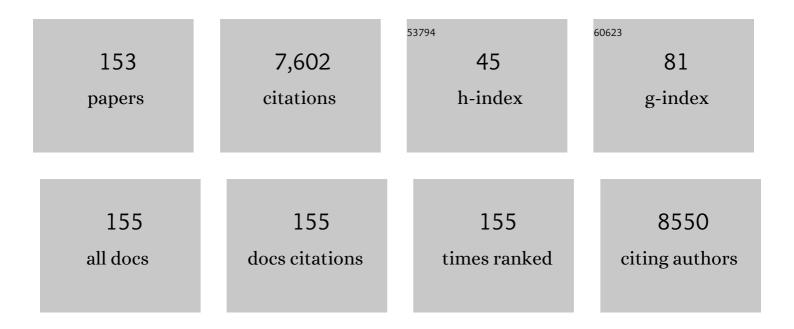
## Yajie Chen

List of Publications by Year in descending order

Source: https://exaly.com/author-pdf/10995775/publications.pdf Version: 2024-02-01



VALLE CHEN

#	Article	IF	CITATIONS
1	Boosted charge transfer and photocatalytic CO2 reduction over sulfur-doped C3N4 porous nanosheets with embedded SnS2-SnO2 nanojunctions. Science China Materials, 2022, 65, 400-412.	6.3	21
2	Fabrication of size-controlled hierarchical ZnS@ZnIn2S4 heterostructured cages for enhanced gas-phase CO2 photoreduction. Journal of Colloid and Interface Science, 2022, 605, 253-262.	9.4	47
3	Efficient charge transfer in cadmium sulfide quantum dot-decorated hierarchical zinc sulfide-coated tin disulfide cages for carbon dioxide photoreduction. Journal of Colloid and Interface Science, 2022, 615, 606-616.	9.4	5
4	Hierarchical CuS@ZnIn <sub>2</sub> S <sub>4</sub> Hollow Double-Shelled p–n Heterojunction Octahedra Decorated with Fullerene C <sub>60</sub> for Remarkable Selectivity and Activity of CO <sub>2</sub> Photoreduction into CH <sub>4</sub> . ACS Applied Materials & Interfaces, 2022, 14, 7888-7899.	8.0	34
5	Emerging magnetodielectric materials for 5G communications: 18H hexaferrites. Acta Materialia, 2022, 231, 117854.	7.9	35
6	Dielectric Constant, Exchange Bias, and Magnetodielectric Effect in CrO2/Cr2O3 Nanostructures. Journal of Superconductivity and Novel Magnetism, 2022, 35, 1719-1725.	1.8	1
7	Sandwich-Structured Hybrid of NiCo Nanoparticles-Embedded Carbon Nanotubes Grafted on C <sub>3</sub> N <sub>4</sub> Nanosheets for Efficient Photodehydrogenative Coupling Reactions. ACS Applied Materials & Interfaces, 2022, 14, 24425-24434.	8.0	14
8	Hierarchical CuCo <sub>2</sub> S <sub>4</sub> Nanoflake Arrays Grown on Carbon Cloth: A Remarkable Bifunctional Electrocatalyst for Overall Water Splitting. ChemElectroChem, 2021, 8, 1134-1140.	3.4	19
9	Cu2O decorated α-Fe2O3/SnS2 core/shell heterostructured nanoarray photoanodes for water splitting. Solar Energy, 2021, 220, 843-851.	6.1	12
10	Hierarchical Co <sub>0.85</sub> Seâ€CdSe/MoSe <sub>2</sub> /CdSe Sandwichâ€Like Heterostructured Cages for Efficient Photocatalytic CO <sub>2</sub> Reduction. Small, 2021, 17, e2100412.	10.0	29
11	Electromagnetic shielding effectiveness of amorphous metallic spheroidal- and flake-based magnetodielectric composites. Journal of Materials Science and Technology, 2021, 83, 256-263.	10.7	13
12	Improved charge separation and carbon dioxide photoreduction performance of surface oxygen vacancy-enriched zinc ferrite@titanium dioxide hollow nanospheres with spatially separated cocatalysts. Journal of Colloid and Interface Science, 2021, 599, 1-11.	9.4	15
13	Sulfur doped In2O3-CeO2 hollow hexagonal prisms with carbon coating for efficient photocatalytic CO2 reduction. Chemical Engineering Journal, 2021, 421, 129968.	12.7	52
14	Enhanced Visibleâ€Light Photoactivities of Perovskiteâ€Type LaFeO <sub>3</sub> Nanocrystals by Simultaneously Doping Er <sup>3+</sup> and Coupling MgO for CO <sub>2</sub> Reduction. ChemCatChem, 2020, 12, 623-630.	3.7	14
15	Recent Progress in Heavy Metal Ion Decontamination Based on Metal–Organic Frameworks. Nanomaterials, 2020, 10, 1481.	4.1	37
16	A Position-Independent Approach to Accurate Measurement of Broadband Electromagnetic Constitutive Parameters of Magnetodielectric Materials. IEEE Transactions on Microwave Theory and Techniques, 2020, 68, 4940-4950.	4.6	10
17	Efficient Separation of Photogenerated Charges in Sandwiched Bi <sub>2</sub> S <sub>3</sub> â^'BiOCl Nanoarrays/BiVO <sub>4</sub> Nanosheets Composites for Enhanced Photocatalytic Activity. ChemCatChem, 2020, 12, 3223-3229.	3.7	5
18	Dual-Mode Light-Emitting Lanthanide Metal–Organic Frameworks with High Water and Thermal Stability and Their Application in White LEDs. ACS Applied Materials & Interfaces, 2020, 12, 18934-18943.	8.0	65

#	Article	IF	CITATIONS
19	Suppressed domain wall damping in planar BaM hexaferrites for miniaturization of microwave devices. Journal of Magnetism and Magnetic Materials, 2020, 514, 167172.	2.3	15
20	Hierarchical ZnO nanorod/ZnFe2O4 nanosheet core/shell nanoarray decorated with PbS quantum dots for efficient photoelectrochemical water splitting. Journal of Alloys and Compounds, 2020, 828, 154449.	5.5	28
21	Hierarchical NiS decorated CuO@ZnFe2O4 nanoarrays as advanced photocathodes for hydrogen evolution reaction. International Journal of Hydrogen Energy, 2020, 45, 6174-6183.	7.1	19
22	Achieving cadmium selenide-decorated zinc ferrite@titanium dioxide hollow core/shell nanospheres with improved light trapping and charge generation for photocatalytic hydrogen generation. Journal of Colloid and Interface Science, 2020, 575, 158-167.	9.4	16
23	Permeability spectra of planar Mâ€ŧype barium hexaferrites with high Snoek's product by twoâ€step sintering. Journal of the American Ceramic Society, 2020, 103, 5076-5085.	3.8	18
24	Controlled synthesis and exceptional photoelectrocatalytic properties of Bi2S3/MoS2/Bi2MoO6 ternary hetero-structured porous film. Journal of Colloid and Interface Science, 2019, 555, 214-223.	9.4	26
25	Clustering effect on permeability spectra of magneto-dielectric composites with conductive magnetic inclusions. Journal of Applied Physics, 2019, 125, .	2.5	10
26	Hierarchical SnS <sub>2</sub> /CuInS <sub>2</sub> Nanosheet Heterostructure Films Decorated with C <sub>60</sub> for Remarkable Photoelectrochemical Water Splitting. ACS Applied Materials & Interfaces, 2019, 11, 9093-9101.	8.0	68
27	Nickel–Cobalt Diselenide Nanosheets Supported on Copper Nanowire Arrays for Synergistic Electrocatalytic Oxygen Evolution. Advanced Materials Interfaces, 2019, 6, 1802052.	3.7	22
28	Concurrent Core Loss Suppression and High Permeability by Introduction of Highly Insulating Intergranular Magnetic Inclusions to MnZn Ferrite. IEEE Magnetics Letters, 2018, 9, 1-5.	1.1	18
29	Ni <sub>2</sub> P Entwined by Graphite Layers as a Low-Pt Electrocatalyst in Acidic Media for Oxygen Reduction. ACS Applied Materials & Interfaces, 2018, 10, 9999-10010.	8.0	34
30	Enhanced charge transfer and separation of hierarchical hydrogenated TiO <sub>2</sub> nanothorns/carbon nanofibers composites decorated by NiS quantum dots for remarkable photocatalytic H <sub>2</sub> production activity. Nanoscale, 2018, 10, 4041-4050.	5.6	39
31	Highly dispersed of Ni0.85Se nanoparticles on nitrogen-doped graphene oxide as efficient and durable electrocatalyst for hydrogen evolution reaction. Electrochimica Acta, 2018, 262, 107-114.	5.2	39
32	Particle-size distribution modified effective medium theory and validation by magneto-dielectric Co-Ti substituted BaM ferrite composites. Journal of Magnetism and Magnetic Materials, 2018, 453, 44-47.	2.3	28
33	Exceptional visible-light photoelectrocatalytic activity of In2O3/In2S3/CdS ternary stereoscopic porous heterostructure film for the degradation of persistent 4-fluoro-3-methylphenol. Applied Catalysis B: Environmental, 2018, 225, 477-486.	20.2	66
34	Hydrogenated Cu <sub>2</sub> OAu@CeO <sub>2</sub> Z-scheme catalyst for photocatalytic oxidation of amines to imines. Catalysis Science and Technology, 2018, 8, 5535-5543.	4.1	23
35	NiSeâ€Ni <sub>0.85</sub> Se Heterostructure Nanoflake Arrays on Carbon Paper as Efficient Electrocatalysts for Overall Water Splitting. Small, 2018, 14, e1800763.	10.0	185
36	Giant Enhancement of Magnetostrictive Response in Directionally-Solidified Fe83Ga17Erx Compounds. Materials, 2018, 11, 1039.	2.9	21

#	Article	IF	CITATIONS
37	Control of Room-Temperature Magnetoelectric Effect via the Initial Electric Phase State in Sr \$_{3}\$Co \$_{2}\$Fe\$_{24}\$ O\$_{41}\$ Hexaferrite. IEEE Magnetics Letters, 2017, 8, 1-4.	1.1	5
38	Cubic quantum dot/hexagonal microsphere ZnIn <sub>2</sub> S <sub>4</sub> heterophase junctions for exceptional visible-light-driven photocatalytic H <sub>2</sub> evolution. Journal of Materials Chemistry A, 2017, 5, 8451-8460.	10.3	176
39	Selfâ€5upported NiS Nanoparticleâ€Coupled Ni <sub>2</sub> P Nanoflake Array Architecture: An Advanced Catalyst for Electrochemical Hydrogen Evolution. ChemElectroChem, 2017, 4, 1341-1348.	3.4	17
40	Enhanced photogenerated carrier separation in CdS quantum dot sensitized ZnFe <sub>2</sub> O <sub>4</sub> /ZnIn <sub>2</sub> S <sub>4</sub> nanosheet stereoscopic films for exceptional visible light photocatalytic H <sub>2</sub> evolution performance. Nanoscale, 2017, 9, 5912-5921.	5.6	76
41	Crystal structure tailored microwave magnetodielectric effect in YbYFeO ceramics. Journal of Alloys and Compounds, 2017, 726, 1030-1039.	5.5	16
42	Tailoring large magnetodielectric response in core/shell CrO2/Cr2O3 nano-rods. Journal of Alloys and Compounds, 2017, 692, 950-954.	5.5	8
43	Single-Point FMR Linewidth Measurement by TE <sub>10</sub> Rectangular Transmission Cavity Perturbation. IEEE Transactions on Microwave Theory and Techniques, 2016, 64, 3772-3780.	4.6	14
44	Hydrogenated TiO2/SrTiO3 porous microspheres with tunable band structure for solar-light photocatalytic H2 and O2 evolution. Science China Materials, 2016, 59, 1003-1016.	6.3	32
45	Magnetic spectra and Richter aftereffect relaxation in CexY3â^'xFe5O12 ferrites. AIP Advances, 2016, 6, 055918.	1.3	5
46	In situ formation of a ZnO/ZnSe nanonail array as a photoelectrode for enhanced photoelectrochemical water oxidation performance. Nanoscale, 2016, 8, 9366-9375.	5.6	52
47	Facile synthesis of well-dispersed Bi2S3 nanoparticles on reduced graphene oxide and enhanced photocatalytic activity. Applied Surface Science, 2016, 378, 231-238.	6.1	49
48	Ferromagnetic resonance induced large microwave magnetodielectric effect in cerium doped Y3Fe5O12 ferrites. Scientific Reports, 2016, 6, 28206.	3.3	28
49	Magnetic Properties of a Highly Textured Barium Hexa-Ferrite Quasi-Single Crystal and Its Application in Low-Field Biased Circulators. Journal of Electronic Materials, 2016, 45, 5069-5073.	2.2	11
50	Enhanced Microwave Absorption of SiO2-Coated Fe0.65Co0.35 Flakes at a Wide Frequency Band (1–18ÂGHz). Journal of Electronic Materials, 2016, 45, 3640-3645.	2.2	12
51	Room temperature magnetoelectric effect of YFeO 3 –Y 3 Fe 5 O 12 ferrite composites. Journal of Alloys and Compounds, 2016, 656, 465-469.	5.5	15
52	Stable mesoporous ZnFe2O4 as an efficient electrocatalyst for hydrogen evolution reaction. Electrochimica Acta, 2016, 190, 186-192.	5.2	43
53	Influence of particle size on the magnetic spectrum of NiCuZn ferrites for electromagnetic shielding applications. Journal of Magnetism and Magnetic Materials, 2016, 401, 1093-1096.	2.3	34
54	Hierarchical Ag/Ag <sub>2</sub> S/CuS Ternary Heterostructure Composite as an Efficient Visible‣ight Photocatalyst. ChemCatChem, 2015, 7, 1684-1690.	3.7	23

#	Article	IF	CITATIONS
55	Visible-Light-Induced Self-Cleaning Property of Bi <sub>2</sub> Ti <sub>2</sub> O <sub>7</sub> -TiO <sub>2</sub> Composite Nanowire Arrays. Langmuir, 2015, 31, 5962-5969.	3.5	40
56	BiFeO3 tailored low loss M-type hexaferrite composites having equivalent permeability and permittivity for very high frequency applications. Journal of Alloys and Compounds, 2015, 630, 48-53.	5.5	63
57	High frequency permeability and permittivity spectra of BiFeO3/(CoTi)-BaM ferrite composites. Journal of Applied Physics, 2015, 117, 17A306.	2.5	11
58	Dual-ion substitution induced high impedance of Co 2 Z hexaferrites for ultra-high frequency applications. Acta Materialia, 2015, 98, 190-196.	7.9	23
59	Single-crystalline Bi <sub>19</sub> Br <sub>3</sub> S <sub>27</sub> nanorods with an efficiently improved photocatalytic activity. CrystEngComm, 2015, 17, 6120-6126.	2.6	17
60	Enhanced microwave absorption of multiferroic Co 2 Z hexaferrite–BaTiO 3 composites with tunable impedance matching. Journal of Alloys and Compounds, 2015, 643, 111-115.	5.5	46
61	Tunable permittivity and permeability of low loss Z + Y-type ferrite composites for ultra-high frequency applications. Journal of Applied Physics, 2015, 117, .	2.5	13
62	One-step synthesis of a hierarchical Bi <sub>2</sub> S <sub>3</sub> nanoflowerIn <sub>2</sub> S <sub>3</sub> nanosheet composite with efficient visible-light photocatalytic activity. CrystEngComm, 2015, 17, 8720-8727.	2.6	38
63	Equilibrium Chemical Disorder at the Surface of a Single-Crystal \${m C1}_{b}\$ NiMnSb Half-Heusler Alloy: Implications for Spintronics. IEEE Magnetics Letters, 2015, 6, 1-4.	1.1	2
64	Hierarchical FeTiO <sub>3</sub> –TiO <sub>2</sub> hollow spheres for efficient simulated sunlight-driven water oxidation. Nanoscale, 2015, 7, 15924-15934.	5.6	50
65	Process optimization and properties of magnetically hard cobalt carbide nanoparticles via modified polyol method. Journal of Alloys and Compounds, 2015, 625, 138-143.	5.5	15
66	Hierarchical MoS2/Bi2MoO6 composites with synergistic effect for enhanced visible photocatalytic activity. Applied Catalysis B: Environmental, 2015, 164, 40-47.	20.2	237
67	Magnetic properties and scale-up of nanostructured cobalt carbide permanent magnetic powders. Journal of Applied Physics, 2014, 115, 17A747.	2.5	14
68	Giant magnetoresistance due to magnetoelectric currents in Sr3Co2Fe24O41 hexaferrites. Applied Physics Letters, 2014, 105, .	3.3	24
69	Low loss factor Co2Z ferrite composites with equivalent permittivity and permeability for ultra-high frequency applications. Applied Physics Letters, 2014, 105, .	3.3	51
70	Nanoscale-Driven Crystal Growth of Hexaferrite Heterostructures for Magnetoelectric Tuning of Microwave Semiconductor Integrated Devices. ACS Nano, 2014, 8, 11172-11180.	14.6	13
71	Magnetic and microwave properties of U-type hexaferrite films with high remanence and low ferromagnetic resonance linewidth. Journal of Applied Physics, 2014, 115, 17A504.	2.5	23
72	Enhanced Photocatalytic Hydrogen Evolution over Hierarchical Composites of ZnIn <sub>2</sub> S <sub>4</sub> Nanosheets Grown on MoS <sub>2</sub> Slices. Chemistry - an Asian Journal, 2014, 9, 1291-1297.	3.3	57

#	Article	IF	CITATIONS
73	Epitaxial growth of 100- <i>î¼</i> m thick <i>M</i> -type hexaferrite crystals on wide bandgap semiconductor GaN/Al2O3 substrates. Journal of Applied Physics, 2014, 115, .	2.5	11
74	High quality Y-type hexaferrite thick films for microwave applications by an economical and environmentally benign crystal growth technique. Applied Physics Letters, 2014, 104, 072411.	3.3	4
75	Effects of intrinsic magnetostriction on tube-topology magnetoelectric sensors with high magnetic field sensitivity. Journal of Applied Physics, 2014, 115, .	2.5	10
76	Hierarchical composites of TiO2 nanowire arrays on reduced graphene oxide nanosheets with enhanced photocatalytic hydrogen evolution performance. Journal of Materials Chemistry A, 2014, 2, 4366-4374.	10.3	112
77	In situ growth of Bi <sub>2</sub> MoO <sub>6</sub> on reduced graphene oxide nanosheets for improved visible-light photocatalytic activity. CrystEngComm, 2014, 16, 842-849.	2.6	80
78	One-pot controlled synthesis of sea-urchin shaped Bi <sub>2</sub> S <sub>3</sub> /CdS hierarchical heterostructures with excellent visible light photocatalytic activity. Dalton Transactions, 2014, 43, 12396-12404.	3.3	67
79	Hierarchical Core–Shell Carbon Nanofiber@ZnIn <sub>2</sub> S <sub>4</sub> Composites for Enhanced Hydrogen Evolution Performance. ACS Applied Materials & Interfaces, 2014, 6, 13841-13849.	8.0	179
80	Growth rate controlled synthesis of hierarchical Bi2S3/In2S3 core/shell microspheres with enhanced photocatalytic activity. Scientific Reports, 2014, 4, 4027.	3.3	108
81	Enhanced Coercivity of CaLaCoâ€Doped SrM Hexaferrites by Microwave alcination Technique. Journal of the American Ceramic Society, 2014, 97, 1873-1877.	3.8	5
82	Thermally driven large magnetoresistance and magnetostriction in multifunctional magnetic FeGa–Tb alloys. Acta Materialia, 2014, 73, 19-26.	7.9	41
83	Synthesis of hierarchical TiO2 nanoflower with anatase–rutile heterojunction as Ag support for efficient visible-light photocatalytic activity. Dalton Transactions, 2013, 42, 11242.	3.3	68
84	Ag–Y2O3:Eu3+ composite nanotubes: synthesis, tunable photoluminescence and surface-enhanced Raman scattering. CrystEngComm, 2013, 15, 7484.	2.6	11
85	Impact of Structural and Magnetic Anisotropies on Microwave Ferrites. Solid State Physics, 2013, , 331-347.	0.5	2
86	Effect of Ambient Aging on Heat-Treated Mechanically Alloyed Mn-Al-C Powders. IEEE Transactions on Magnetics, 2013, 49, 3372-3374.	2.1	8
87	Vertically aligned anatase TiO2 nanowire bundle arrays: Use as Pt support forÂcounter electrodes in dye-sensitized solar cells. Journal of Power Sources, 2013, 238, 350-355.	7.8	14
88	Hierarchical flake-like Bi2MoO6/TiO2 bilayer films for visible-light-induced self-cleaning applications. Journal of Materials Chemistry A, 2013, 1, 6961.	10.3	102
89	Hierarchical Composite of Ag/AgBr Nanoparticles Supported on Bi <sub>2</sub> MoO <sub>6</sub> Hollow Spheres for Enhanced Visibleâ€Light Photocatalytic Performance. ChemPlusChem, 2013, 78, 117-123.	2.8	58
90	Hierarchical CuS hollow nanospheres and their structure-enhanced visible light photocatalytic properties. CrystEngComm, 2013, 15, 5144.	2.6	106

#	Article	IF	CITATIONS
91	In situ controlled growth of ZnIn2S4 nanosheets on reduced graphene oxide for enhanced photocatalytic hydrogen production performance. Chemical Communications, 2013, 49, 2237.	4.1	171
92	Crystallographically textured self-biased W-type hexaferrites for X-band microwave applications. Journal of Applied Physics, 2013, 113, .	2.5	31
93	Giant enhancement in the magnetostrictive effect of FeGa alloys doped with low levels of terbium. Applied Physics Letters, 2013, 102, 222409.	3.3	53
94	Enhanced photocatalytic activity and upconversion luminescence of flowerlike hierarchical Bi <sub>2</sub> MoO <sub>6</sub> microspheres by Er <sup>3+</sup> doping. Journal of Materials Research, 2012, 27, 1471-1475.	2.6	16
95	Controlled synthesis of thorny anatase TiO <sub>2</sub> tubes for construction of Ag–AgBr/TiO <sub>2</sub> composites as highly efficient simulated solar-light photocatalyst. Journal of Materials Chemistry, 2012, 22, 2081-2088.	6.7	84
96	Magneto-electric effects on Sr Z-type hexaferrite at room temperature. Journal of Applied Physics, 2012, 111, .	2.5	29
97	Room temperature solution synthesis of hierarchical bow-like Cu2O with high visible light driven photocatalytic activity. RSC Advances, 2012, 2, 2875.	3.6	38
98	Consequences of magnetic anisotropy in realizing practical microwave hexaferrite devices. Journal of Magnetism and Magnetic Materials, 2012, 324, 3393-3397.	2.3	22
99	In situ controlled growth of well-dispersed gold nanoparticles in TiO <sub>2</sub> nanotube arrays as recyclable substrates for surface-enhanced Raman scattering. Dalton Transactions, 2012, 41, 1020-1026.	3.3	54
100	Controlled synthesis and luminescence properties of rhombic NaLn(MoO4)2 submicrocrystals. CrystEngComm, 2012, 14, 5015.	2.6	35
101	Permeability spectra of Co2Z hexaferrite compacts produced via a modified aqueous co-precipitation technique. Journal of Magnetism and Magnetic Materials, 2012, 324, 3719-3722.	2.3	22
102	In situ synthesis and photoluminescence of Eu3+ doped Y(OH)3@β-NaYF4 core–shell nanotubes. Chemical Communications, 2011, 47, 8019.	4.1	21
103	Numeric Simulations of a Novel Wideband Electromagnetic Band Gap Metamaterial Utilizing Oriented Cobalt-Substituted Z-Type Barium Hexaferrites. IEEE Magnetics Letters, 2011, 2, 0500104-0500104.	1.1	16
104	Facile solvothermal synthesis of hierarchical flower-like Bi <sub>2</sub> MoO <sub>6</sub> hollow spheres as high performance visible-light driven photocatalysts. Journal of Materials Chemistry, 2011, 21, 887-892.	6.7	427
105	Tunable fringe magnetic fields induced by converse magnetoelectric coupling in a FeGa/PMN-PT multiferroic heterostructure. Journal of Applied Physics, 2011, 110, .	2.5	16
106	Self Biased Y-Junction Circulator at \${m K}_{m u}\$ Band. IEEE Microwave and Wireless Components Letters, 2011, 21, 292-294.	3.2	64
107	Electronic tuning of magnetic permeability in Co2Z hexaferrite toward high frequency electromagnetic device miniaturization. Applied Physics Letters, 2011, 98, .	3.3	43
108	3D hierarchical flower-like TiO2 nanostructure: morphology control and its photocatalytic property. CrystEngComm, 2011, 13, 2994.	2.6	237

#	Article	IF	CITATIONS
109	Converse Magnetoelectric Effect in a Fe-Ga/PMN-PT Laminated Multiferroic Heterostructure for Field Generator Applications. IEEE Transactions on Magnetics, 2011, 47, 4050-4053.	2.1	13
110	Quasi-one-dimensional miniature multiferroic magnetic field sensor with high sensitivity at zero bias field. Applied Physics Letters, 2011, 99, .	3.3	48
111	Solvothermal Synthesis, Characterization, and Formation Mechanism of a Single‣ayer Anatase TiO <sub>2</sub> Nanosheet with a Porous Structure. European Journal of Inorganic Chemistry, 2011, 2011, 754-760.	2.0	22
112	Magnetoelectric effect in crystallographically textured BaTiO3 films deposited on ferromagnetic metallic glass foils. Journal of Applied Physics, 2011, 109, .	2.5	24
113	Microwave magnetoelectric coupling and ferromagnetic resonance frequency tuning of a Co <mml:math <br="" xmlns:mml="http://www.w3.org/1998/Math/MathML">display="inline"&gt;<mml:mrow><mml:msub><mml:mrow /&gt;<mml:mrow><mml:mn></mml:mn></mml:mrow></mml:mrow </mml:msub></mml:mrow></mml:math> MnSb/GaAs/PZN-PT	3.2	26
114	heterostructure. Physical Review B, 2011, 83, . Dynamic response of converse magnetoelectric effect inÂaÂPMN-PT-based multiferroic heterostructure. Applied Physics A: Materials Science and Processing, 2010, 100, 1149-1155.	2.3	20
115	Efficient visible light-induced degradation of phenol on N-doped anatase TiO2 with large surface area and high crystallinity. Applied Surface Science, 2010, 256, 3740-3745.	6.1	29
116	Preparation and Characterization of Pureâ€Phase Co <sub>2</sub> Y Ferrite Powders via a Scalable Aqueous Coprecipitation Method. Journal of the American Ceramic Society, 2010, 93, 2994-2997.	3.8	18
117	Electric field controlled magnetic hysteresis loops in a Metglas®/PMN–PT heterostructure. Journal Physics D: Applied Physics, 2010, 43, 155001.	2.8	12
118	Electrically controlled magnetization switching in a multiferroic heterostructure. Applied Physics Letters, 2010, 97, 052502.	3.3	63
119	Large microwave tunability of GaAs-based multiferroic heterostructure for applications in monolithic microwave integrated circuits. Journal Physics D: Applied Physics, 2010, 43, 495002.	2.8	1
120	Large tunability of Néel temperature by growth-rate-induced cation inversion in Mn-ferrite nanoparticles. Applied Physics Letters, 2009, 94, 113109.	3.3	29
121	The effect of boron addition on the atomic structure and microwave magnetic properties of FeGaB thin films. Journal of Applied Physics, 2009, 105, 07A323.	2.5	7
122	Time domain analyses of the converse magnetoelectric effect in a multiferroic metallic glass-relaxor ferroelectric heterostructure. Applied Physics Letters, 2009, 95, 182501.	3.3	28
123	Large converse magnetoelectric coupling in FeCoV/lead zinc niobate-lead titanate heterostructure. Applied Physics Letters, 2009, 94, .	3.3	45
124	Giant magnetodielectric effect and magnetic field tunable dielectric resonance in spinel MnZn ferrite. Applied Physics Letters, 2009, 94, .	3.3	53
125	Topochemical growth of textured polycrystalline barium hexaferrite from oriented antiferromagnetic α-FeOOH nanorods. Nanotechnology, 2009, 20, 445606.	2.6	15
126	Low Bias Field Hexagonal Y-Type Ferrite Phase Shifters at \${K}_{U}\$-Band. IEEE Transactions on Magnetics, 2009, 45, 4179-4182.	2.1	17

#	Article	IF	CITATIONS
127	Giant Electric Field Tuning of Magnetic Properties in Multiferroic Ferrite/Ferroelectric Heterostructures. Advanced Functional Materials, 2009, 19, 1826-1831.	14.9	387
128	Recent advances in processing and applications of microwave ferrites. Journal of Magnetism and Magnetic Materials, 2009, 321, 2035-2047.	2.3	696
129	Realization of Far From Equilibrium Cation Distributions in Ferrites. IEEE Transactions on Magnetics, 2009, 45, 666-669.	2.1	4
130	Effect of Mn doping on magnetic and transport properties of SrRuO3 perovskite. Solid State Communications, 2008, 145, 259-262.	1.9	7
131	Perpendicularly Oriented Polycrystalline BaFe <sub>11.1</sub> Sc <sub>0.9</sub> O <sub>19</sub> Hexaferrite with Narrow FMR Linewidths. Journal of the American Ceramic Society, 2008, 91, 2952-2956.	3.8	79
132	Microstructural, Magnetic and Microwave Properties of Large Area BaFe\$_{12}\$O\$_{19}\$ Thick Films (\$>!100 mu\$m) Deposited on /a-SiO\$_{2}\$/Si and /a-Al\$_{2}\$O\$_{3}\$/Si Substrates. IEEE Transactions on Magnetics, 2008, 44, 4571-4577.	2.1	12
133	Magnetocaloric effect in 4d itinerant ferromagnet SrRuO3. Journal of Alloys and Compounds, 2008, 459, 51-54.	5.5	9
134	Realization of hexagonal barium ferrite thick films on Si substrates using a screen printing technique. Journal Physics D: Applied Physics, 2008, 41, 095006.	2.8	23
135	Structural, Magnetic, and Microwave Properties of BaFe\$_{10.5}\$Mn\$_{1.5}\$O\$_{19}\$ Thin Films. IEEE Transactions on Magnetics, 2008, 44, 2966-2969.	2.1	3
136	Atomic Scale Design and Control of Cation Distribution in Hexagonal Ferrites. Physical Review Letters, 2008, 101, 067201.	7.8	31
137	Giant magnetoelectric coupling and E-field tunability in a laminated Ni2MnGa/lead-magnesium-niobate-lead titanate multiferroic heterostructure. Applied Physics Letters, 2008, 93, 112502.	3.3	73
138	Studies of magnetic entropy change and phase transitions in SrRu1â^'xMnxO3 perovskite. Journal of Applied Physics, 2008, 103, 07B303.	2.5	4
139	Magnetic and atomic structure parameters of Sc-doped barium hexagonal ferrites. Journal of Applied Physics, 2008, 103, .	2.5	20
140	Synthesis of ordered arrays of multiferroic NiFe2O4-Pb(Zr0.52Ti0.48)O3 core-shell nanowires. Applied Physics Letters, 2007, 90, 152501.	3.3	118
141	Pulsed laser ablation deposition of nanocrystalline exchange-coupled Ni11Co11Fe67â^'xZr7B4Cux (x=0,1) films for planar inductor applications. Journal of Applied Physics, 2007, 101, 09M519.	2.5	6
142	Competition between ferromagnetism and antiferromagnetism: origin of large magnetoresistance in polycrystalline SrRu1â^'xMnxO3(0≤â‰⊉). Journal of Physics Condensed Matter, 2007, 19, 266211.	1.8	25
143	Large magnetocaloric effect in chromium dioxide with second-order phase transition. Journal Physics D: Applied Physics, 2007, 40, 3243-3247.	2.8	9
144	Low-loss barium ferrite quasi-single-crystals for microwave application. Journal of Applied Physics, 2007, 101, 09M501.	2.5	63

#	Article	IF	CITATIONS
145	Magnetic semiconducting anatase TiO2â^`î´ grown on (100) LaAlO3 having magnetic order up to 880K. Journal of Magnetism and Magnetic Materials, 2007, 309, 171-175.	2.3	46
146	Screen printed thick self-biased, low-loss, barium hexaferrite films by hot-press sintering. Journal of Applied Physics, 2006, 100, 043907.	2.5	61
147	Oriented barium hexaferrite thick films with narrow ferromagnetic resonance linewidth. Applied Physics Letters, 2006, 88, 062516.	3.3	100
148	Microwave and magnetic properties of self-biased barium hexaferrite screen printed thick films. Journal of Applied Physics, 2006, 99, 08M904.	2.5	51
149	Oxygen-defect-induced magnetism to 880 K in semiconducting anatase TiO2â^îfilms. Journal of Physics Condensed Matter, 2006, 18, L355-L361.	1.8	256
150	Ba-hexaferrite films for next generation microwave devices (invited). Journal of Applied Physics, 2006, 99, 08M911.	2.5	175
151	Enhanced magnetoresistance and surface state of CrO2 particles improved by chemical process. Journal of Magnetism and Magnetic Materials, 2006, 307, 134-138.	2.3	6
152	A potential oxide for magnetic refrigeration application: CrO2particles. Journal of Physics Condensed Matter, 2006, 18, L559-L566.	1.8	18
153	Room temperature magnetism in semiconducting films of ZnO doped with ferric ions. Journal of Applied Physics, 2006, 99, 08M109.	2.5	26